Design and Implementation of a Novel MSK-based Frequency-Domain SWIPT Multiplexing Scheme

Rahul Gupta, Konstantinos Ntougias, and Ioannis Krikidis
Department of Electrical and Computer Engineering, University of Cyprus
Email: {gupta.rahul, ntougias.konstantinos, krikidis.ioannis}@ucy.ac.cy

***Abstract*—In this paper, we propose a novel frequency-domain simultaneous wireless information and power transfer (FD-SWIPT) waveform which allows for rectifiers based on local oscillators (LO) and eliminates the need for receive (demultiplexing) filters. This is achieved via appropriate multiplexing a multitone energy signal with a minimum shift keying (MSK) data signal. We analytically derive the average error probability for a point-to-point link in the presence of i.i.d. Rayleigh fading, additive white Gaussian noise, and multitone interference. The performance of the proposed waveform is evaluated via numerical simulations, assuming either a LOs-based receiver or a power splitting (PS)-based one for comparison purposes. The simulation results show that the proposed scheme substantially increases both the data rate and the harvested energy in comparison with conventional PS-SWIPT at the cost of negligible performance loss in data detection. Finally, the proposed concept is experimentally validated in a realistic indoor propagation environment.**

***Index Terms*—Frequency-domain simultaneous wireless information and power transfer (FD-SWIPT), minimum shift keying (MSK) modulation, multitone energy signal, waveform design, experimental validation.**

I. Introduction

Simultaneous wireless information and power transfer (SWIPT) integrates wireless energy supply in the downlink to prolong the lifetime of power-constrained end devices, such as wireless sensors and Internet-of-Things (IoT) nodes, via energy harvesting (EH) [1]. In practice, though, the receiver commonly orthogonalizes the information decoding (ID) and EH processes in the power [2] or time [3] domain, due to implementation issues. This sharing of resources among the information and energy streams results in performance loss.

Frequency-domain (FD) SWIPT represents an alternative that addresses this issue via frequency multiplexing of the information and energy streams at the transmitter and separation of them at the receiver with the assistance of complementary filters. In [4], the transmitter superimposes a direct current (DC) energy signal onto an orthogonal frequency division multiplexing (OFDM) data signal. A corresponding frequency splitting receiver architecture that makes use of a 3-port circulator and a notch filter to separate the data and energy signals is proposed in [5]. In [6], a multitone energy signal is embedded on a continuous-phase modulation (CPM) data signal. In this work, the authors use a combination of peak and notch filters to separate the information and energy signals over an additive white Gaussian noise (AWGN) channel. They also utilize a linear rectifier based on local oscillators (LO) operating at the tones' frequencies instead of diodes.

The main drawback of FD-SWIPT schemes is the requirement for using receive filters, since practical filters are non-ideal and near-ideal filters are expensive. In this paper, we design a novel FD-SWIPT waveform, wherein a multitone energy signal is frequency multiplexed with a minimum-shift keying (MSK) data signal. The use of the former is dictated by spectral regulations, which might prevent the transmission of a single high-power tone, while the utilization of the latter is motivated by its spectral characteristics [7]. Specifically, by placing the tones of the energy signal at the spectral nulls and/or low-power sub-bands that characterize the power spectral density (PSD) of MSK signals, we minimize the interference incurred to the data signal by the energy signal, thus ensuring similar information transfer performance with the MSK-only case and simplifying the separation of these signals at the receiver. In fact, with appropriate multitone signal design, we can avoid the use of notch/peak filters.

An example of the proposed MSK-SWIPT waveform is illustrated in Fig. 1. In this case, an energy signal with $N = 4$ tones f_i $(i = 1, \ldots, N)$ placed in the frequency interval $[0.45/T_b, \ldots, 0.75/T_b]$, where T_b is the bit duration, is superimposed on an MSK signal with first frequency null at $ft_b = 0.75$. The tone spacing is $\Delta = 0.1/T_b$ and the i-th tone corresponds to a signal-to-interference-ratio (SIR) SIR_i.

The unique contributions of this paper that set it apart from similar studies, such as the work in [6], are listed below:

- we derive the average error probability of the MSK-SWIPT waveform for a point-to-point wireless link in the presence of i.i.d. Rayleigh fading, AWGN, and multitone interference;
- we evaluate via numerical simulations the performance of MSK-SWIPT with either an LOs-based receiver without notch/peak filters or a power splitting (PS)-based one (for comparison purposes), using various EH models in the latter scenario to capture the non-linear behavior of the EH circuit; and
- we validate the proposed concept via measurements performed in a realistic indoor propagation environment.

Numerical simulations highlight the substantial performance gains of MSK-FD-SWIPT, in terms of the achieved data rate and harvested power, over MSK-PS-SWIPT. Furthermore, the simulation results indicate that the performance loss in MSK detection attributed to the application of the proposed SWIPT scheme is negligible.

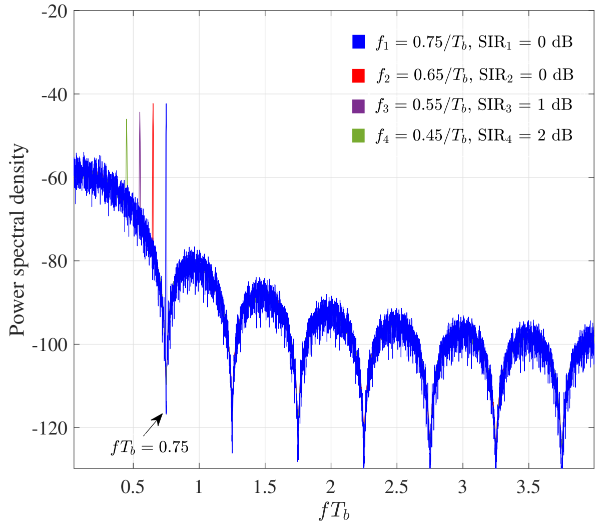

Fig. 1. PSD of MSK modulated information signal with a superimposed four-tones energy signal.

The paper is structured as follows: Section II introduces the system model as well as the considered non-linear EH models and performance metrics. Section III focuses on the error rate analysis of the proposed MSK-FD-SWIPT waveform as well as on the design of the multitone energy signal. Section IV describes the experimental validation setup and demonstration and presents the numerical simulation results. Finally, Section V provides our conclusions. The mathematical proofs are given in the Appendix.

II. System Model

A. Transmitter

The block diagram of the MSK-SWIPT transmitter and receiver is depicted in Fig. 2. At the transmitter, information is MSK modulated. Also, a multitone energy signal is generated, with controllable frequency and amplitude for each tone. Next, the modulated and energy signals are filtered, amplified, and combined. Finally, the composite signal is transmitted.

Therefore, the transmitted MSK-SWIPT signal $x(t)$ consists of two components, namely, an MSK modulated information transfer (IT) signal and a multitone power transfer (PT) signal. This signal can be expressed as

$$x(t) = x_{\text{IT}}(t) + x_{\text{PT}}(t). \tag{1}$$

The MSK modulated information signal is defined in terms of orthonormal basis functions $\phi_1(t)$ and $\phi_2(t)$ as [7]

$$x_{\text{IT}}(t) = s_1(t)\phi_1(t) + s_2(t)\phi_2(t), \tag{2}$$

where

$$\phi_1(t) = \sqrt{\frac{2}{T_b}}\cos\left(\frac{\pi t}{2T_b}\right)\cos(w_c t), \quad -T_b \le t \le T_b, \tag{3a}$$

$$\phi_2(t) = \sqrt{\frac{2}{T_b}}\sin\left(\frac{\pi t}{2T_b}\right)\sin(w_c t), \quad 0 \le t \le 2T_b. \tag{3b}$$

$(s_1, s_2) = \left(\sqrt{E_b}, \pm\sqrt{E_b}\right)$ in Eq. (1) refers to the coordinates of the message points, with E_b denoting the bit energy, whereas T_b in Eq. (2) is the bit duration and w_c represents the (angular) carrier frequency.

The PSD of the MSK modulated signal is expressed as [8]

$$S(f) = \frac{32E_b}{\pi^2}\left[\frac{\cos(2\pi f T_b)}{1-(4fT_b)^2}\right]^2. \tag{4}$$

From Eq. (4), we can compute the spectral null frequencies of the MSK modulated signal as follows:

$$\frac{32E_b}{\pi^2}\left[\frac{\cos(2\pi f T_b)}{1-(4fT_b)^2}\right]^2 = 0 \Rightarrow fT_b = \frac{2n+1}{4}, \tag{5}$$

where the first null is at $n = 1$, i.e., $fT_b = 0.75$.

The multitone PT signal can be written as

$$x_{\text{PT}}(t) = \sum_{i=1}^{N} \alpha_i \cos\left(w_c t + w_i t + \theta_i\right), \tag{6}$$

where α_i and w_i denote the tones' amplitudes and frequencies, which constitute the design parameters of the PT signal; N represents the number of tones; and θ_i refers to the phases, which are arbitrary.

B. Receiver

Assuming transmission over a quasi-static i.i.d. Rayleigh fading channel with AWGN, the received signal is given by

$$y(t) = hx(t) + n(t), \tag{7}$$

where h denotes the i.i.d. zero-mean complex Gaussian channel's impulse response with unit variance and $n(t)$ represents the AWGN with variance N_0.

As shown in Fig. 2, in the LOs-based receiver, the received signal is forwarded to the rectifier in the EH branch, which is comprised by LOs operating at the frequencies of the energy signal's tones, and to the MSK demodulator in the ID branch.

In the PS-based receiver, on the other hand, a portion ρ of the received signal's power is allocated to the former stream and the remaining portion $(1-\rho)$ is allocated to the latter stream, where $0 < \rho < 1$ is the PS factor. Thus, the received signal at the input of the EH and ID branches is given by

$$y_{\text{PT}}(t) = \sqrt{\rho}\, y(t);\ \ y_{\text{IT}}(t) = \sqrt{(1-\rho)}\, y(t) + n_c(t), \tag{8}$$

where $n_c(t)$ is the i.i.d. zero-mean complex Gaussian circuit noise with variance N_c that is attributed to the baseband conversion of the received RF signal for ID purposes. The rectifier in this case consists of one or more diodes in some arrangement and it is followed by a low-pass filter (LPF) that smooths the ripple of the output voltage.

C. Harvested Energy

The average power of the received RF signal is given by:

$$\mathcal{P}_r = \mathbb{E}\left\{|y(t)|^2\right\} = \mathbb{E}\left\{|h|^2 P + N_0\right\}, \tag{9}$$

where P is the transmit power. For the case of the LOs-based receiver, the DC harvested power is simply $\mathcal{P}_{\text{DC}} = \mathcal{P}_r$.

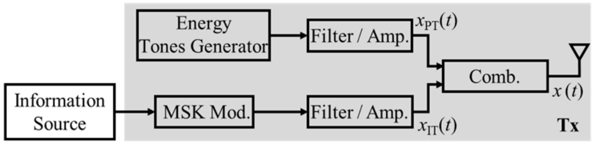

(a) MSK-SWIPT transmitter.

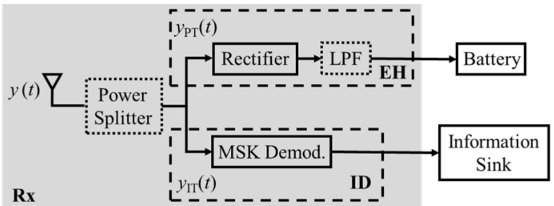

(b) MSK-SWIPT receiver.

Fig. 2. Block diagram of the MSK-SWIPT transmitter (Tx) and receiver (Rx).

Let us now turn our attention to the PS-based receiver. The average power at the input of the rectifier is $\mathcal{P}_{\mathrm{EH}} = \rho \mathcal{P}_r$. Considering a piecewise linear EH model, the DC harvested power can be written as [9]

$$\mathcal{P}_{\mathrm{DC}} = \begin{cases} 0, & \mathcal{P}_{\mathrm{EH}} < \mathcal{P}_{\mathrm{th}_1}; \\ \eta \left(\mathcal{P}_{\mathrm{EH}} - \mathcal{P}_{\mathrm{th}_1}\right), & \mathcal{P}_{\mathrm{th}_1} \leq \mathcal{P}_{\mathrm{EH}} \leq \mathcal{P}_{\mathrm{th}_2}; \\ \eta \mathcal{P}_{\mathrm{th}_2}, & \mathcal{P}_{\mathrm{EH}} > \mathcal{P}_{\mathrm{th}_2}, \end{cases} \tag{10}$$

where $\eta \in [0, 1]$ is the energy conversion efficiency, while $\mathcal{P}_{\mathrm{th}_1}$ and $\mathcal{P}_{\mathrm{th}_2}$ denote the sensitivity and saturation thresholds of the rectifier circuit, respectively. Considering instead a parametric non-linear EH model that is based on the logistic (sigmoidal) function, the harvested power is given by [10]

$$\mathcal{P}_{\mathrm{DC}} = \frac{\mathcal{P}_{\mathrm{th}_2}\left(\Omega_r - \Omega\right)}{1 - \Omega}, \tag{11a}$$

$$\Omega_r = \frac{1}{1 + e^{-a_1 (\mathcal{P}_{\mathrm{EH}} - a_2)}}; \ \Omega = \frac{1}{1 + e^{a_1 a_2}}, \tag{11b}$$

where the parameters a_1 and a_2 are constants related to the specifications of the EH circuit. We note that the use of PS and a diodes-based rectifier negatively affects EH.

D. Data Rate

The instantaneous power of the received signal (excluding AWGN) at the ID branch of the LOs-based and PS-based receivers is given by

$$\mathcal{P}_{\mathrm{r,LO}} = |h|^2 P; \ \mathcal{P}_{\mathrm{r,PS}} = (1 - \rho) |h|^2 P. \tag{12}$$

Thus, the instantaneous receive signal-to-noise-ratio (SNR) is expressed as

$$\mathrm{SNR}_{\mathrm{LO}} = \frac{|h|^2 P}{N_0 + N_c}; \ \mathrm{SNR}_{\mathrm{PS}} = \frac{|h|^2 P}{N_0 + \frac{N_c}{(1-\rho)}}. \tag{13}$$

In both cases, the ergodic capacity is given by $R = \mathbb{E}\left\{\log_2\left(1 + \mathrm{SNR}\right)\right\}$. We notice in Eq. (13) the negative impact of PS on the SNR and, therefore, on the ergodic capacity.

III. Error Rate Analysis

Let's initially assume an AWGN channel, where $y(t) = x(t) + n(t)$. The integrator output for the I-branch at the ID circuit of the MSK-SWIPT receiver is expressed as

$$r_I = \int_{-T_b}^{T_b} \sqrt{\frac{2}{T_b}} \cos\left(\frac{\pi t}{2T_b}\right) \cos\left(w_c t\right) y(t) dt. \tag{14}$$

After simplification (see Appendix A), we obtain

$$r_I = \sqrt{E_b}\big(1 + A_I\big) + N_0, \tag{15}$$

where

$$A_I = \sum_{i=1}^{N} \frac{4 \cos\theta_i \cos(2\pi f_i T_b)}{\pi \sqrt{\mathrm{SIR}_i}\left[1 - \left(4 f_i T_b\right)^2\right]}. \tag{16}$$

In Eq. (16), $\mathrm{SIR}_i = A^2/\alpha_i^2$, where A denotes the amplitude of the carrier signal. We have $\mathrm{SNR} = E_b/N_0 = A^2 T_b / 2N_0$. Thus, the probability of error for the I-branch is obtained as

$$P_{e_I} = \frac{1}{2}\mathrm{erfc}\left[\sqrt{\mathrm{SNR}}\big(1 + A_I\big)\right]. \tag{17}$$

Similarly, the integrator output for the Q-branch is given as

$$r_Q = \int_{0}^{2T_b} \sqrt{\frac{2}{T_b}} \sin\left(\frac{\pi t}{2T_b}\right) \sin\left(w_c t\right) y(t) dt, \tag{18}$$

and the probability of error for the Q-branch is obtained as (see Appendix A)

$$P_{e_Q} = \frac{1}{2}\mathrm{erfc}\left[\sqrt{\mathrm{SNR}}\big(1 - A_Q\big)\right], \tag{19}$$

where

$$A_Q = \sum_{i=1}^{N} \frac{2\left[\sin(4\pi f_i T_b + \theta_i) + \sin\theta_i\right]}{\pi \sqrt{\mathrm{SIR}_i}\left[1 - \left(4 f_i T_b\right)^2\right]}. \tag{20}$$

The overall probability of error is $P_e = P_{e_I} + P_{e_Q}/2$.

Next, we find the error probability in the presence of standard i.i.d. Rayleigh fading. Under this context, the probability density function (PDF) of h is given by $f_{\mathcal{H}}(h) = 2he^{-h^2}$. Hence, the PDF of fading power $b = |h|^2$ is obtained as $f_{\mathcal{B}}(b) = e^{-b}$. From Eq. (17), we can find the average probability of error over Rayleigh fading for the I-branch as

$$P_{c_I} = \int_{0}^{\infty} \frac{1}{2}\mathrm{erfc}\left[\sqrt{b}\sqrt{\mathrm{SNR}}\big(1 + A_I\big)\right] e^{-b} db. \tag{21}$$

After solving the above integral (see Appendix B), we get

$$P_{c_I} = \frac{1}{2}\left[1 - \sqrt{\frac{\Gamma_I}{\Gamma_I + 1}}\right], \tag{22}$$

where $\Gamma_I = \mathrm{SNR}\big(1 + A_I\big)^2$.

Similarly for the Q-branch, by defining $\Gamma_Q = \mathrm{SNR}\big(1 - A_Q\big)^2$, we obtain

$$P_{c_Q} = \frac{1}{2}\left[1 - \sqrt{\frac{\Gamma_Q}{\Gamma_Q + 1}}\right]. \tag{23}$$

Thus, the overall average probability of error over a Rayleigh fading channel is obtained as

$$P_c = \frac{1}{4}\left[2 - \sqrt{\frac{\Gamma_I}{\Gamma_I + 1}} - \sqrt{\frac{\Gamma_Q}{\Gamma_Q + 1}}\right]. \tag{24}$$

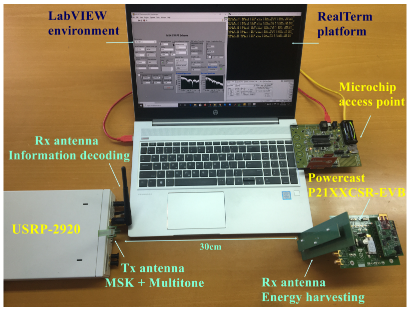

Fig. 3. MSK-SWIPT setup testbed.

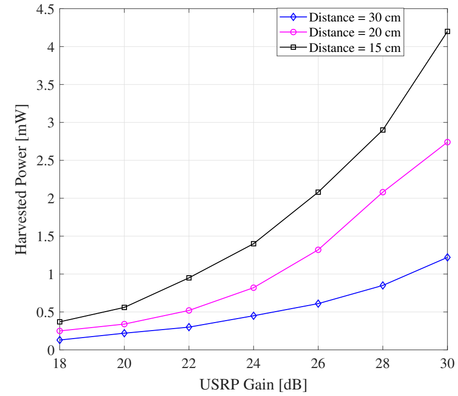

Fig. 4. Harvested power vs. transmit gain for different Tx-Rx distances.

IV. Experiments and Simulations

A. Experimental Validation

The validity of the proposed SWIPT technique was experimentally demonstrated in an indoor propagation environment. The testbed is shown in Fig. 3. Two USRP-2920 hardware units [11] act as Tx and ID circuit, respectively, while a Powercast P21XXCSR-EVB evaluation board [12] acts as EH circuit. LabVIEW software is installed at both the Tx and the Rx for performing signal processing operations. The Rx consists also of a microchip access point module that reads and disseminates the harvested power values and RealTerm software that displays these data. As shown in Fig. 4, the harvested power increases with higher transmit gain and/or shorter propagation distance, as expected.

B. Numerical Simulations

In this section, we evaluate the performance of MSK-SWIPT through numerical simulations. We assume an i.i.d. Rayleigh fading channel with unit variance. The RF carrier frequency, sampling rate, and oversampling factor are set to 915 MHz, 4 Ms/s, and 4, respectively. The phases θ_i follow a uniform distribution in $[0, 2\pi]$, while the tone spacing is $\Delta = 0.1$. The tones are placed at the spectral null or/and low-power sub-band. The energy conversion efficiency, circuit sensitivity, saturation threshold, and noise variance at the receiver are set to 0.8, -20 dBm, 10 dBm, and -35 dBm, respectively. The EH circuit specifications are $a_1 = 1500$ and $a_2 = 0.0022$ [13]. We consider 10^5 iterations with 10000 symbols in each.

Fig. 5 illustrates the achievable rate-energy (R-E) regions of MSK-SWIPT with a 3-tone PT signal for the cases where an LOs-based receiver or a PS-based receiver is utilized. Different EH models are considered in the latter scenario, as discussed in Section II-C. For comparison fairness, we scale the power at the EH and ID branches of the LOs-based receiver according to the power scaling noticed in the PS-based receiver. The simulation results are obtained by varying ρ from 0 to 1 when the average SNR is 10 dB. It is noted that MSK-SWIPT significantly outperforms PS-SWIPT due to the direct RF-to-DC conversion achieved by using a bank of LOs.

Fig. 6 plots both the simulated and the theoretical probability of error of MSK-SWIPT versus the SNR. It is observed that the MSK-SWIPT waveform can achieve the same error performance as the MSK signal alone. It is also noticed that as we shift the tones of the PT signal to the high-power sub-bands of the MSK signal, the probability of error starts to increase due to the higher multitone interference, as expected.

V. Conclusions

A novel MSK-SWIPT waveform has been proposed in this paper. The average error probability was derived in the presence of Rayleigh fading. Numerical simulations have shown that by appropriately selecting the frequency components of the multitone energy signal, we can increase the data rate and harvested power in comparison to the PS-SWIPT approach and maintain the error rate performance of pure MSK, without the need for using receive filters. The proposed design was experimentally validated in an indoor propagation environment.

Acknowledgements

This work was co-funded by the European Regional Development Fund and the Republic of Cyprus through the Research and Innovation Foundation, under the projects INFRASTRUCTURES/1216/0017 (IRIDA) and EXCELLENCE/1918/0377 (PRIME). It has also received funding from the European Research Council (ERC) under the EU's Horizon 2020 research and innovation programme (Grant agreement No. 81981).

Appendix A

Substituting $x_{\mathrm{IT}}(t)$ and $x_{\mathrm{PT}}(t)$ in Eq. (14), we obtain

$$r_I = \sqrt{E_b} + \sum_{i=1}^{N} \frac{\alpha_i}{\sqrt{2T_b}} \int_{-T_b}^{T_b} \cos(w_i t + \theta_i) \cos\left(\frac{\pi t}{2T_b}\right) + N_0. \tag{25}$$

After simplifying the above integral, we have

$$\begin{aligned} r_I &= \sqrt{E_b} + \sum_{i=1}^{N} \frac{4\alpha_i \pi \sqrt{T_b} \cos\theta_i \cos(w_i T_b)}{\sqrt{2}\left[\pi^2 - 4w_i^2 T_b^2\right]} + N_0 \\ &= \sqrt{E_b}\big(1 + A_I\big) + N_0, \end{aligned} \tag{26}$$

where A_I is given in Eq. (16).

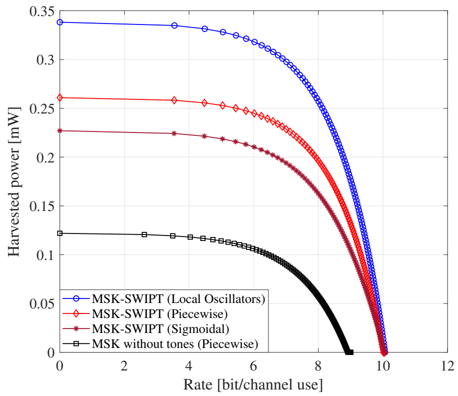

Fig. 5. R-E region of MSK-SWIPT for different receivers and EH models.

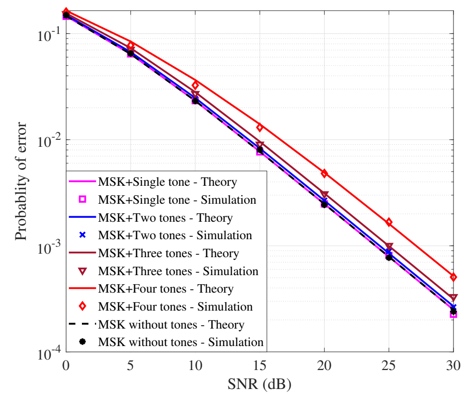

Fig. 6. Probability of error versus SNR: Theoretical vs. simulation results.

Similarly, for the integrator output in the Q-branch we get

$$\begin{aligned} r_Q &= \sqrt{E_b} - \sum_{i=1}^{N} \frac{\alpha_i \pi \sqrt{2T_b}\left[\sin(2w_i T_b + \theta_i) + \sin\theta_i\right]}{\left[\pi^2 - 4w_i^2 T_b^2\right]} + N_0 \\ &= \sqrt{E_b}\big(1 - A_Q\big) + N_0, \end{aligned} \tag{27}$$

where A_Q is defined in Eq. (20).

Finally, the overall probability of error over AWGN with multitone interference is obtained as

$$\begin{aligned} P_e = &\frac{1}{4}\mathrm{erfc}\left[\sqrt{\mathrm{SNR}}\big(1 + A_I\big)\right] \\ &+ \frac{1}{4}\mathrm{erfc}\left[\sqrt{\mathrm{SNR}}\big(1 - A_Q\big)\right]. \end{aligned} \tag{28}$$

Appendix B

From Eq. (17), we obtain the average probability of error over Rayleigh fading for the I-branch as

$$\begin{aligned} P_{c_I} &= \int_0^\infty \frac{1}{2}\mathrm{erfc}\left[\sqrt{b}\sqrt{\mathrm{SNR}}\big(1 + A_I\big)\right] e^{-b} db \\ &= \frac{1}{2}\int_0^\infty \mathrm{erfc}\left(\sqrt{b\Gamma_I}\right) e^{-b} db \\ &\overset{v = b\Gamma_I}{=} \frac{1}{2\Gamma_I}\int_0^\infty \mathrm{erfc}\left(\sqrt{v}\right) e^{-\frac{v}{\Gamma_I}} dv \\ &= \frac{1}{2} - \frac{1}{2\sqrt{\pi}}\int_0^\infty e^{-v\left(\frac{1+\Gamma_I}{\Gamma_I}\right)} v^{-1/2} dv \\ &\overset{u = v\left(\frac{1+\Gamma_I}{\Gamma_I}\right)}{=} \frac{1}{2} - \frac{1}{2\sqrt{\pi}}\sqrt{\frac{\Gamma_I}{1+\Gamma_I}}\int_0^\infty e^{-u} u^{-1/2} du, \end{aligned} \tag{29}$$

where $\Gamma_I = \mathrm{SNR}\big(1 + A_I\big)^2$. Since $\int_0^\infty e^{-u}u^{-1/2}du = \sqrt{\pi}$, we have

$$P_{c_I} = \frac{1}{2}\left[1 - \sqrt{\frac{\Gamma_I}{\Gamma_I + 1}}\right]. \tag{30}$$

Similarly from Eq. (19), we express the average probability of error over Rayleigh fading for the Q-branch as

$$\begin{aligned} P_{c_Q} &= \int_0^\infty \frac{1}{2}\mathrm{erfc}\left[\sqrt{b}\sqrt{\mathrm{SNR}}\big(1 - A_Q\big)\right] e^{-b} db \\ &= \frac{1}{2}\left[1 - \sqrt{\frac{\Gamma_Q}{\Gamma_Q + 1}}\right], \end{aligned} \tag{31}$$

where $\Gamma_Q = \mathrm{SNR}\big(1 - A_Q\big)^2$. The overall average probability of error is obtained as $P_c = P_{c_I} + P_{c_Q}/2$.

References

[1] B. Clerckx, R. Zhang, R. Schober, D. W. K. Ng, D. I. Kim, and H. V. Poor, "Fundamentals of wireless information and power transfer: From RF energy harvester models to signal and system designs," *IEEE J. Sel. Areas Commun.*, vol. 37, no. 1, pp. 4–33, Jan. 2019.

[2] L. Liu, R. Zhang, and K. Chua, "Wireless information and power transfer: A dynamic power splitting approach," *IEEE Trans. Commun.*, vol. 61, no. 9, pp. 3990–4001, Sep. 2013.

[3] T. D. Ponnimbaduge Perera, D. N. K. Jayakody, S. K. Sharma, S. Chatzinotas, and J. Li, "Simultaneous wireless information and power transfer (SWIPT): Recent advances and future challenges," *IEEE Commun. Surveys Tuts.*, vol. 20, no. 1, pp. 264–302, 1st Quart. 2018.

[4] M. N. Khormuji, B. M. Popović, and A. G. Perotti, "Enabling SWIPT via OFDM-DC," in *Proc. IEEE Wireless Commun. Netw. Conf.*, Apr. 2019, pp. 1–6.

[5] H. H. Jang, K. W. Choi, and D. I. Kim, "Novel frequency-splitting SWIPT for overcoming amplifier nonlinearity," *IEEE Wireless Commun. Lett.*, vol. 9, no. 6, pp. 826–829, Feb. 2020.

[6] A. G. Perotti, M. N. Khormuji, and B. M. Popović, "Simultaneous wireless information and power transfer by continuous-phase modulation," *IEEE Commun. Lett.*, vol. 24, no. 6, pp. 1294–1298, Mar. 2020.

[7] S. Pasupathy, "Minimum shift keying: A spectrally efficient modulation," *IEEE Commun. Mag.*, vol. 17, no. 4, pp. 14–22, Jul. 1979.

[8] J. G. Proakis and M. Salehi, *Communication Systems Engineering*. Second edition, by Prentice-Hall, Inc. Upper Saddle River, New Jersey, © 2002.

[9] W. Liu, X. Zhou, S. Durrani, and P. Popovski, "SWIPT with practical modulation and RF energy harvesting sensitivity," in *Proc. IEEE Int. Conf. Commun.*, May 2016, pp. 1–7.

[10] E. Boshkovska, D. W. K. Ng, N. Zlatanov, and R. Schober, "Practical non-linear energy harvesting model and resource allocation for SWIPT systems," *IEEE Commun. Lett.*, vol. 19, no. 12, pp. 2082–2085, Sep. 2015.

[11] National Instruments Universal Software Radio Peripheral USRP platform, ©2020 National Instruments Corp., Austin. [Online]. Available: http://www.ni.com

[12] Powercast, Power Management IC Development Tools, ©2020 Powercast Corp., US. [Online]. Available: https://www.powercastco.com

[13] Y. Dong, M. J. Hossain, and J. Cheng, "Performance of wireless powered amplify and forward relaying over nakagami-m fading channels with nonlinear energy harvester," *IEEE Commun. Lett.*, vol. 20, no. 4, pp. 672–675, Feb. 2016.